

– 1 –

# Numerical Analysis of Magnetic Field Amplification by Turbulence

by

**Hongsong Chou**

*Harvard-Smithsonian Center for Astrophysics, Cambridge, MA 02138, U.S.A.*

*chou5@fas.harvard.edu*

Received \_\_\_\_\_; accepted \_\_\_\_\_

## ABSTRACT

We apply a Fourier spectral numerical method to 3D incompressible MHD turbulence with a magnetic Prandtl number  $Pr \geq 1$ . We examine the processes by which an initially weak, large-scale seed magnetic field and an initially weak, small-scale, impulse-like seed magnetic field are amplified. We find that in both cases the magnetic energy spectrum grows at all scales. The growth rates at different amplification stages are analyzed. For a large-scale seed magnetic field, the magnetic energy density grows as  $\sim t^2$  for the first few turbulence eddy turnover times, followed by a dynamic growth stage, where nonlinear interactions between different scales of the turbulence contribute to an exponential growth rate that is largely determined by the turbulence eddy turnover time. For a seed magnetic field that is initially set up at a small scale in the turbulence, during the kinematic development stage, the growth rate of magnetic energy is  $\propto 1/\tau_{max}$ , where  $\tau_{max}$  is the eddy turnover time of the smallest eddies of the turbulence. The kinematic growth stage is followed by a dynamic growth stage, where nonlinearity plays important role. During such dynamic growth stage, the growth rate of total magnetic energy is determined by both the magnetic energy amplification within the turbulence inertial range and that within the turbulence dissipation range.

*Subject headings:* MHD turbulence, Dynamo

## 1. Introduction

Astrophysical magnetic field has often been observed on much larger scales than the scales of astrophysical turbulence. The connection between the generation of large-scale magnetic field and the turbulence of much smaller scales has been contemplated by astrophysicists for many decades. Mean-field electrodynamics (MFE, see Moffatt 1978 or Krause & Rädler 1980), among other theories, employs a two-scale approach to the problem. It suggests that the helical turbulent motions of astrophysical plasma may align small-scale magnetic field so that an observable, large-scale magnetic field can be formed. Because MFE is largely a linear theory, its applicability to nonlinear phenomena such as the solar or interstellar turbulence has been questioned ever since the introduction of this theory. Some early criticism of MFE was discussed by Piddington (1975). He argued that kinematic solar dynamo theories do not account for the removal of the large amounts of flux generated each solar cycle. Recent objections to dynamo action have their root in the problem of small-scale magnetic fields. The amplification of seed magnetic field in galaxies has been considered by Kulsrud & Anderson (1992). The magnetic Prandtl number, defined as  $Pr = \nu/\lambda$  where  $\nu$  is the molecular viscosity and  $\lambda$  the magnetic resistivity, is much greater than 1 in the interstellar medium of galaxies. Kulsrud & Anderson predict that the growth rate of an initially weak, small-scale magnetic field in  $Pr \gg 1$  systems will be  $\propto 1/\tau_{max}$ , where  $\tau_{max}$  being the eddy turnover time of the smallest turbulent eddies. Because  $\tau_{max}$  is very small in astrophysical turbulence, the growth rate of the small-scale magnetic field will be large. They then argue that because of such fast amplification of magnetic energy at small scales, the turbulence may be reduced dramatically in a short period of time, so that it is unable to amplify the magnetic field at scales much larger than the turbulent dissipation scale. The recent work by Kinney *et al.* (2000, see also Cowley 2000) also criticizes the galactic dynamo theory by arguing that because the galactic plasma

has a very large magnetic Prandtl number, any small-scale seed magnetic field will grow quickly to lock the velocity field in a shear motion pattern, where the dissipation term in the momentum equation,  $\nu \nabla^2 \mathbf{U}$ , is balanced by the Lorentz force term,  $\mathbf{B} \cdot \nabla \mathbf{B}$ . Here  $\mathbf{U}$  and  $\mathbf{B}$  are the velocity field and the magnetic field.

This work is motivated by the studies of Kulsrud & Anderson and Kinney *et al.* We noticed that the work by Kulsrud & Anderson can be valid only for the kinematic development of the magnetic field, as back reaction of the magnetic field on the velocity field was not considered in their governing equations. Therefore, their prediction that the magnetic field at large scales may not grow after the velocity field is quenched at small scales needs examination. We also noticed that the simulation by Kinney *et al.* is for 2D MHD, which can be very different from the case of 3D MHD. Moreover, they focused their research on those scales that are smaller than the velocity dissipation scales, and did not include the inertial range of the turbulence. To further understand the physics of magnetic field amplification by turbulence and its application to 3D astrophysical systems, we carried out a numerical study of incompressible 3D MHD systems. With our numerical model, we study the amplification of initially weak, large-scale and small-scale seed magnetic field by turbulence. Unlike the theoretical analysis of Kulsrud & Anderson, our numerical study is not restricted to the kinematic development stage of the MHD system. Rather, we can also study the effects of back reaction. Unlike the numerical work by Kinney *et al.* (2000), we include an inertial range in our numerical model, and study whether or not the magnetic field within the inertial range will grow, especially when the magnetic field beyond the turbulence dissipation scale ( $l_{v,D}$ ) grows and significantly modifies the velocity field near  $l_{v,D}$ .

The structure of this paper is as follows: we introduce our numerical model in section 2; sections 3 and 4 are devoted to the detailed numerical analysis of magnetic energy

spectrum development for a large-scale seed field and a small-scale seed field, respectively; the physical implications and applications of our numerical results are discussed in section 5; conclusions and suggestions for future work are given in section 6. Our numerical study is different from those of Brandenburg (2000) and Cho & Vishniac (2000) in the following ways: first, not like the work of Cho & Vishniac, in most of our simulations, we have a magnetic Prandtl number  $Pr = 3$ , so that the velocity dissipation scale is larger than the magnetic dissipation scale; second, there is no scale separation as the one discussed in Brandenburg (2000); third, although Brandenburg (2000) studied cases of various magnetic Prandtl numbers, the initial conditions for the simulation runs in that work are different from those in our work; therefore, the physical processes considered in that work and ours are different.

In this work, we distinguish four scales. We denote the size of turbulence energy containing eddies as  $L$ .  $L$  is also called the outer scale or the integral scale of the turbulence. We denote the dissipation scales of the velocity field and the magnetic field as  $l_{v,D}$  and  $l_{b,D}$ , respectively. For turbulence of large kinetic Reynolds number, we have  $L \gg l_{v,D}$ . In Fourier space, we introduce two wave numbers that correspond to  $l_{v,D}$  and  $l_{b,D}$ :  $k_{v,D} \sim 1/l_{v,D}$  and  $k_{b,D} \sim 1/l_{b,D}$ . In some of our simulation runs, we have  $k_{b,D} > k_{v,D}$ , i.e., the magnetic dissipation scale is smaller than the velocity dissipation scale. This is consistent with a magnetic Prandtl that is greater than 1. In other simulation runs, we have  $Pr = 1$ . Another scale is the so-called “ensemble average scale”, which is denoted by  $\Gamma \gg L$  and over which we calculate averaged quantities,  $\langle \cdot \rangle$  (or  $\overline{\cdot}$ ). Finally, we denote the scale of the whole physical system as  $S$ , which is the typical scale for the variations of averaged quantities  $\langle \cdot \rangle$  (or  $\overline{\cdot}$ ). What we mean by “large scale” in the following sections is the scale  $\sim S$ . So we have the relation  $S \gg \Gamma \gg L \gg l_{v,D} \geq l_{b,D}$ . In our model, there are two large-scale quantities,  $\overline{\mathbf{B}}$  and  $\overline{\mathbf{V}}$ . We assume both of these quantities are constant, i.e.,  $S \rightarrow \infty$ . We

set our reference frame to that moving at  $\bar{\mathbf{V}}$  and henceforth omit terms of  $\bar{\mathbf{V}}$ . To aid our discussion, we decompose the total magnetic field into two parts:  $\mathbf{B} = \bar{\mathbf{B}} + \mathbf{b}$ , where  $\mathbf{b}$  is the fluctuating component of  $\mathbf{B}$ . To make our discussion easy to follow, throughout the paper we will use a few terms and notations, which will be introduced as we proceed. They are also listed in Table 1. Readers may refer to this table for further clarification.

## 2. The Numerical Model

We focus on the incompressible MHD equations, which are solved numerically using the standard Fourier spectral method. The nonlinear terms are evaluated by a pseudo-spectral procedure. Let  $\mathbf{B}$  and  $\mathbf{U}$  be the magnetic field and the velocity field, respectively. Under an external forcing term  $\mathcal{F}$ , the undimensionalized incompressible MHD equations can be written as (with Einstein summation convention)

$$\left(\partial_t - R_e^{-1} \nabla^2\right) U_i = \partial_j (-p \delta_{ij} - U_i U_j + B_i B_j) + \mathcal{F}_i, \quad (1)$$

$$\left(\partial_t - R_m^{-1} \nabla^2\right) B_i = \partial_j (U_i B_j - B_i U_j), \quad (2)$$

$$\partial_i U_i = \partial_j B_j = 0. \quad (3)$$

where  $R_e$  and  $R_m$  are the kinematic and magnetic Reynolds numbers and defined as

$$R_e = \frac{v_{rms} L}{\nu}, \quad R_m = \frac{v_{rms} L}{\lambda}. \quad (4)$$

Here  $v_{rms}$  is the root-mean-square of the velocity field,  $L$  the integral scale of the turbulence,  $\nu$  the molecular viscosity,  $\lambda$  the magnetic resistivity. Note that we have already written  $B$  in units of  $\sqrt{4\pi\rho}$  after we divide both sides of the momentum equation and the induction equation by density  $\rho$ . If we use a hat,  $\hat{\cdot}$ , to denote discrete Fourier transform, and  $\otimes$  to denote convolution, the above equations in Fourier space are

$$\left(\partial_t + \nu k^2\right) \hat{U}_j = P_{jl} \left[ ik_m \left( -\hat{U}_l \otimes \hat{U}_m + \hat{B}_l \otimes \hat{B}_m \right) + \hat{\mathcal{F}}_l \right], \quad (5)$$

$$(\partial_t + \lambda k^2) \hat{B}_j = P_{jl} \left[ ik_m (\hat{U}_l \otimes \hat{B}_m - \hat{U}_m \otimes \hat{B}_l) \right], \quad (6)$$

$$k_m \hat{U}_m = k_j \hat{B}_j = 0. \quad (7)$$

Here  $\mathbf{P}$  is the projection operator defined as  $P_{jl} = \delta_{jl} - \frac{k_j k_l}{k^2}$ . In our simulation, we treat the system as a cube  $[0, 2\pi) \times [0, 2\pi) \times [0, 2\pi)$ . The Cartesian coordinate of a grid point can be written as  $x_l = \frac{2\pi}{N}l, y_m = \frac{2\pi}{N}m, z_n = \frac{2\pi}{N}n$ , for  $l, m, n = 0, 1, 2, \dots, N - 1$ . A point in Fourier space has coordinates  $k_s = s, k_p = p, k_q = q$ , for  $s, p, q = -\frac{N}{2}, -\frac{N-1}{2}, \dots, \frac{N}{2} - 1$ .

Equations (5), (6) and (7) are numerically solved with the standard Fourier pseudo-spectral method. Equations (5) and (6) are treated as ordinary differential equations for  $\hat{U}$  and  $\hat{B}$ . With the projection operator  $\mathbf{P}$ , the divergence free condition (7) will be satisfied for  $t > 0$  as long as  $\hat{U}$  and  $\hat{B}$  are divergence free at  $t = 0$ . All our simulations start from divergence free initial conditions. We employ a second-order Runge-Kutta (RK2) method to advance equations (5) and (6) in time. We can exploit the advantage of using RK2 in the following two aspects. First, an integral factor can be easily introduced with the transform

$$\mathcal{U}_m(t) = \hat{U}_m(\mathbf{k}, t) e^{-\nu k^2 t}, \mathcal{B}_m(t) = \hat{B}_m(\mathbf{k}, t) e^{-\lambda k^2 t}. \quad (8)$$

Second, aliasing errors can be reduced by introducing positive and negative random phase shifts at the first and second stages of RK2, respectively (Machiels & Deville, 1998). The forcing term used in our simulation is a combination of the one used by Chen *et al.* (1993a) and the one used by Brandenburg (2000), with slight modification. Chen *et al.* employed a forcing term that maintains the energy density values at  $k = 1$  and  $k = 2$  so that the energy spectrum of velocity field always follows Kolmogoroff  $k^{-5/3}$  law at  $k = 1$  and  $k = 2$ . In Brandenburg's simulation, he injected helical waves of random phases at  $k = 5$ . Because our simulations start from an established hydrodynamic turbulence, we first use the forcing by Chen *et al.* to obtain a fully developed pure hydrodynamic turbulence. Such fully developed turbulent velocity field is taken as the initial velocity field for the following MHD

turbulence simulation. For all the MHD turbulence simulation runs, the forcing function has the form

$$\hat{\mathcal{F}}(0.5 < |\mathbf{k}| \leq 1.5) = \mathcal{F}_c + \mathcal{F}_b. \quad (9)$$

That is, the force works only within the shell  $S_1 : 0.5 < |\mathbf{k}| \leq 1.5$ . Here  $\mathcal{F}_c$  is a forcing term that is similar to the one adopted by Chen *et al.* It is calculated by multiplying the velocity components within shell  $S_1$  by a factor,  $\gamma > 1$ , so that before a new step of integration starts, the kinetic energy density within this shell is reset to  $E_1 = 0.24$ . Phases of the velocity components within the shell are not changed. This forcing is equivalent as lengthening the velocity vector within shell  $S_1$  by a factor  $\gamma - 1$ . Denote the increment of a velocity vector under force  $\mathcal{F}_c$  as  $\delta\mathbf{v} = \mathbf{R} + i\mathbf{I}$ , where  $\mathbf{R}, \mathbf{I}$  are the real and imaginary parts of  $\delta\mathbf{U}$ . In a few runs of our simulation, we need to inject kinetic helicity into the turbulence. To do this with  $\mathcal{F}_c$ , we tune the angle between  $\mathbf{R}$  and  $\mathbf{I}$  so that they remain perpendicular to each other. Because kinetic helicity at  $\mathbf{k}$  can be calculated as  $H(\mathbf{k}) = 2\mathbf{k} \cdot \mathbf{R} \times \mathbf{I}$ , in doing so, we inject kinetic helicity into the turbulence.

The forcing term  $\mathcal{F}_c$  maintains the energy level at the forcing scale so that the fluctuation in the energy development history can be small; therefore, the growth stages of both the kinetic energy and the magnetic energy can be studied carefully and accurately. However, this force does not introduce random phases into the velocity field. To be more realistic about the forcing in our simulation, we also use the forcing term  $\mathcal{F}_b$ , derived from the forcing function used by Brandenburg (2000), as a secondary forcing function to introduce random phases into the velocity field.  $\mathcal{F}_b$  has the form

$$\mathcal{F}_b(\mathbf{k}) = \mathcal{F}_0 \frac{\mathbf{k} \times (\mathbf{k} \times \hat{\mathbf{e}}) - i|\mathbf{k}|(\mathbf{k} \times \hat{\mathbf{e}})}{2k^2 \sqrt{1 - (\mathbf{k} \cdot \hat{\mathbf{e}}^2)/k^2}} \cos(\phi(t)). \quad (10)$$

Here  $\mathcal{F}_0 < 1$  is a factor adjusted at each time step so that the kinetic energy density within shell  $S_1$  fluctuates within 5% of  $E_1$ .  $\hat{\mathbf{e}}$  is an arbitrary unit vector in Fourier space.

$\phi(t)$  is a random phase. Note that  $\mathcal{F}(\mathbf{k})^* = \mathcal{F}(-\mathbf{k})$  so it is real, and it is helical in that  $\mathcal{F} \cdot \nabla \times \mathcal{F} = -k\mathcal{F}^2 < 0$ , i.e., it has maximum helicity. Because  $\mathcal{F}_b$  is tuned in such way that it only contributes to 5% of the kinetic energy at the forcing scale,  $F_b$  can be considered as a perturbation to  $\mathcal{F}_c$ . Therefore, the advantage of using (9) as the forcing term is three fold: to avoid strong fluctuations of kinetic and magnetic energy density with time, to introduce random phases to the velocity field, and to maintain the kinetic helicity at certain level.

In order to study the non-unit Prandtl number case, we adopt the following hyper-viscosity and hyper-diffusivity:  $-\nu_7 k^{14} \hat{\mathbf{U}}$  and  $-\lambda_7 k^{14} \hat{\mathbf{B}}$ . The dissipation scale of the velocity field is calculated with  $k_{v,D} = \left( \frac{\varepsilon_v}{\nu_h^3} \right)^{\frac{1}{6h-2}}$  (Machiels & Deville, 1998). Here  $h = 7$  is the order of the hyper-viscosity in our simulations.  $\varepsilon_v$  is the mean dissipation rate of the velocity field and is calculated using the formula  $\varepsilon_v = 2\nu_h \sum_k k^{2h} E_v(k)$ , with  $h = 7$ .  $E_v(k)$  is the kinetic energy spectrum.  $k_{b,D}$  is defined in a very similar way as the one  $k_{v,D}$  is defined above. With  $\nu_7 = 5.0 \times 10^{-16}$  and  $\lambda_7 = 3 \times 10^{-20}$  we have the dissipation scales of velocity field and magnetic field as  $k_{v,D} \approx 13$ ,  $k_{b,D} \approx 28$ , respectively, so that the Prandtl number is  $Pr = \left( \frac{k_{b,D}}{k_{v,D}} \right)^{4/3} \approx 3$ . In many other studies (see Brandenburg 2000), the magnetic Prandtl number is defined as the ratio of molecular viscosity to magnetic resistivity. Because we apply hyper-viscosity in most of our simulations, the magnetic Prandtl number used in this work can be considered as an “effective” magnetic Prandtl number, i.e., a ratio inferred from the measured dissipative cutoff wavenumbers.

A 1D version of our code is used to solve the nonlinear Burger’s equation (see section 6.1 of Canuto *et al.* 1988) and the numerical results match exactly the analytic results. If we impose a strong uniform magnetic field and a small disturbance of velocity field, a pair of Alfvén waves are numerically generated, both propagating along the uniform magnetic field but in opposite directions. This is exactly predicted by linearized incompressible MHD equations. Finite amplitude MHD waves are also produced in our numerical simulations (see

section 10.1 of Moffatt, 1978). Our code is also used to study hydrodynamic turbulence with normal dissipation. With the forcing given by (9), the flows reach a statistically stationary state in five to ten large eddy turnover times. In Figure 1, we plot the kinetic energy spectra of two different pure hydrodynamic turbulence simulation runs with normal dissipation. The kinetic energy spectrum is calculated as  $E_v(k) = \frac{1}{2} \sum_{k=0.5}^{k+0.5} \hat{v}(k')^2$ . The magnetic energy spectrum shown in next few sections is calculated as  $E_b(k) = \frac{1}{2} \sum_{k=0.5}^{k+0.5} \hat{b}(k')^2$ . In Figure 1,  $R_\Lambda = v_{rms} \Lambda / \nu$  is the Taylor micro-scale Reynolds number.  $\Lambda$  is the Taylor micro-scale defined by  $\Lambda = \sqrt{15\nu v_{rms}^2 / \epsilon}$ , where  $\epsilon$  is the rate of dissipation of hydrodynamic kinetic energy per unit mass (Chen *et al.* 1993b). For  $R_\Lambda = 43$ , the exponential falloff starts around  $k \sim 6.5$ , while for  $R_\Lambda = 70$ , the falloff starts around  $k \sim 11$ . Both cases exhibit a Kolmogoroff  $k^{-5/3}$  inertial range. With a hyper-viscosity, the turbulence in stationary state will have a energy spectrum that deviates from a Kolmogoroff  $k^{-5/3}$  inertial range. Rather, the spectrum will be flatter than  $k^{-5/3}$ , as shown in numerous simulations (Michiels & Deville, 1998). We plot the kinetic energy spectrum with the hyper-viscosity  $\nu_7 = 5.0 \times 10^{-16}$  in Figure 1. The spectrum in the inertial range follows a power law of  $\sim k^{-1.2}$ . In Table 2, we have listed the parameters of all the simulation runs that we have done for this work. The resolution of our simulations is (64)<sup>3</sup>.

### 3. Amplification of a large-scale seed magnetic field by the turbulence

The amplification of an initially weak, large-scale magnetic field is studied by imposing a constant magnetic field along  $y$ -direction,  $\bar{\mathbf{B}} = \bar{B} \hat{\mathbf{y}}$  with  $\bar{B} = 0.0316$ , into a homogeneous, isotropic and stationary hydrodynamic turbulence under the forcing of (9). The magnetic energy density associated with this initial field is  $\bar{E}_B = 5 \times 10^{-4}$ . Because the turbulence will stretch  $\bar{\mathbf{B}}$ , magnetic field at  $k \geq 1$  will be generated. If the magnetic field is weak,

its back reaction on the velocity field is small; therefore, the turbulence maintains its stationarity until the magnetic field grows strong enough to alter the flows. The growth rate of magnetic field due to the presence of a constant  $\bar{\mathbf{B}}$  with negligible back reaction can be estimated as follows. The induction equation can be written as

$$\partial_t \mathbf{b} = (\bar{\mathbf{B}} \cdot \nabla) \mathbf{U} + \lambda \nabla^2 \mathbf{b}. \quad (11)$$

Therefore, shortly after the start of the simulation, i.e., during the first few eddy turnover times, the magnetic energy spectrum within the inertial range can be calculated as

$$|\hat{\mathbf{b}}(\mathbf{k})|^2 \approx t^2 \bar{B}^2 k^2 |\hat{\mathbf{U}}(\mathbf{k})|^2. \quad (12)$$

If the kinetic energy spectrum follows  $|\hat{\mathbf{U}}(k)|^2 \propto k^{-p}$ , we have  $|\hat{\mathbf{b}}(\mathbf{k})|^2 \propto k^{-p+2}$ . Figure 2 shows the energy spectra of the velocity field and the magnetic field at  $0.1\tau_{eddy}$  after the start of simulation. The kinetic energy spectrum changes little, while the magnetic energy spectrum in the inertial range follows a power law of  $k^{0.77}$ , as predicted. To show how fast the magnetic energy grows in this stage, we calculate the following quantity

$$\beta(t) = \frac{\Delta E_b}{\Delta t} \frac{1}{E_b} \sim \frac{2}{t} \quad (13)$$

for all  $k$ 's as well as the total magnetic energy.  $\beta(t)$  can be considered as an *instantaneous* growth rate. It is an explicit function of and varies with time. From equation (13), we find that  $\beta(t)$  should not be a function of  $k$ , and this is clearly shown in the left panel of Figure 3, where we plot  $\beta(t)$  at different  $k$ 's. At different  $k$ 's,  $\beta(t)$  is roughly the same, and decrease with time. Near dissipation scales,  $\beta(t)$  decreases with time slightly faster than those within the inertial range, and this is due to the strong dissipation at large  $k$ 's, i.e., the dissipation term in (11) becomes important. In the right panel of Figure 3, we plot the averaged value (over  $k$ ) of  $\beta(t)$ , and it behaves like  $\frac{2}{t}$  shortly after the start of simulation, but decreases faster than  $\frac{2}{t}$  as the strength of  $\mathbf{b}$  grows to be comparable with the strength of  $\bar{\mathbf{B}}$ . This

confirms equation (13). The deviation of the averaged  $\beta(t)$  from  $\frac{2}{t}$  after  $t = 4$  becomes more and more prominent as the nonlinear interaction between the velocity field and the growing magnetic field becomes stronger and stronger. This is shown in Figures 4 and 5. From Figure 4, we find that the growth of the magnetic energy density follows four stages. Stage 1 starts from the beginning of the simulation till  $t = 3$ , during which the magnetic energy density grows as  $t^2$ . This is a linear stage in that the line stretching of  $\bar{\mathbf{B}}$  by the velocity field contributes to most of the growth of the magnetic energy, while the velocity field changes little. During stage 2 that lasts from  $t = 4$  till  $t = 16$ , it grows exponentially with a growth rate  $\beta = 0.1$ . The velocity field is suppressed dramatically by the end of stage 1 and at the beginning of stage 2. Figure 4 shows that the kinetic energy density drops by 25% during this period. After the growth of magnetic energy enters the exponential stage, the loss of kinetic energy slows down. Within stage 2, the velocity field loses 5% of its initial energy at  $t = 0$ . The slowdown of the energy loss of velocity field is due to the existence of a forcing, which injects energy at  $0.5 < |\mathbf{k}| \leq 1.5$  so that the  $E_v(0.5 < |\mathbf{k}| \leq 1.5)$  is maintained at  $0.240 \pm 0.012$ . Because the nonlinear interaction between the velocity field and the magnetic field is strongest near the velocity dissipation scale  $k_{v,D}$ , the velocity at small scale is suppressed most, which can be seen from Figure 5. The kinetic energy density at  $k_{v,D} = 13$  drops an order of magnitude from  $t = 0.31$  to  $t = 9.42$ . Therefore, the continuing growth of the total magnetic energy during stage 2 should be attributed to the energy input from the forcing scale and the velocity line stretching within the inertial range. During stage 2, the dominant terms in the induction equation within the inertial range is the line stretching term  $\mathbf{b} \cdot \nabla \mathbf{U}$ , and this is because the fluctuating component  $\mathbf{b}$  of the total magnetic field has grown greater than the imposed  $\bar{\mathbf{B}}$ . The nonlinear interaction between  $\mathbf{U}$  and  $\mathbf{b}$ , and between  $\mathbf{b}$  at different scales provides a self-excitation of  $\mathbf{b}$  that is independent of  $\bar{\mathbf{B}}$  and is capable of exponentially amplifying  $\mathbf{b}$ . Such an exponential

growth rate should be determined by the statistical properties of the velocity field. In our simulation, the largest integral length that the largest eddy circles around can be calculated as  $L = 2\pi \sum_k k^{-1} E_v(k) / \sum_k E_v(k)$ . The rms velocity of the turbulence can be estimated as  $v_{rms} = \sqrt{\frac{2}{3} \sum_k E_v(k)}$ . Within stage 2, we found that the temporal average of  $L$  (denoted by  $\langle L \rangle_t$ ) is  $\langle L \rangle_t \approx 4.62$ , and the temporal average of  $v_{rms}$  (denoted by  $\langle v_{rms} \rangle_t$ ) is  $\langle v_{rms} \rangle_t \approx 0.52$ . Therefore,  $1/\tau_{eddy} = \langle v_{rms} \rangle_t / \langle L \rangle_t = 0.11 \approx \beta$ , which is consistent with the theoretical prediction of Parker (1979).

After the exponential growth stage, magnetic energy density growth enters a near saturation stage from  $t = 16$  to  $t = 30$ , where the growth is further slowed down. During this stage, the magnetic energy at small scales almost stops growing, while at large scales the magnetic field continues to grow. For the saturation stage, magnetic energy density fluctuates around 0.33, while the kinetic energy density fluctuates around 0.4.

The growth of magnetic structures can be seen from Figure 6, where we plotted isosurfaces of the magnetic field strength,  $|\mathbf{B}| \equiv 2.5 \langle |\mathbf{B}| \rangle$ . Here  $\langle |\mathbf{B}| \rangle$  is the spatial mean of the magnitude of the magnetic field. The isosurface at a time shortly after the start of the simulation is shown in panel (a) of Figure 6. At this time point, the magnetic field consists of mostly small-scale structures. The structures shown in panel (a) occupy 3.5% of the whole system and are distributed quite evenly in space. However, at a later stage of the development, the magnetic field develops structures that span scales that are close to the forcing scale,  $k \approx 1$ , in the system. This is shown in panel (b) at  $t = 31.4$  of the saturation stage. Tube-like structures that span the whole simulation box can be clearly seen.

In our simulation of Run A, the kinetic helicity, calculated as  $\langle \mathbf{v} \cdot \nabla \times \mathbf{v} \rangle$  as a function of time, has a value of  $H_v = -0.13 \pm 0.04$ . Most of the kinetic helicity comes from the forcing scale, as the force is helical. The normalized kinetic helicity is

$H_v / (\omega_{rms} \cdot v_{rms}) \approx -0.13/0.74 \cdot 0.51 = 0.27 \pm 0.08$ . Such helical flow will generate a dynamo  $\alpha$ -effect and the  $\alpha$  coefficient can be estimated as  $\alpha \sim -\frac{\tau_{cor}}{3} < \mathbf{v} \cdot \nabla \times \mathbf{v} > \sim 0.05$ , where  $\tau_{cor}$  is the correlation time of velocity field and is measured to be  $\tau_{cor} \sim 1.0$ . A growth rate of the magnetic energy density due to such a dynamo  $\alpha$ -effect can be estimated as  $\beta_\alpha \sim 2\alpha/L \sim 0.02$ , which is smaller than the growth rate in the second stage,  $\beta = 0.1$ . Therefore, it is not clearly evident from this study that the dynamo  $\alpha$ -effect in the moderately helical flow of our simulation is capable of driving the exponential growth of magnetic field in stage 2. Cho and Vishniac (2000) have done recent numerical simulations and also claim that a dynamo  $\alpha$ -effect may play much less important roles in amplifying magnetic field in turbulent flows than the turbulent line stretching effect. One should also notice that the dynamo theory of mean-field electrodynamics requires scale separation between the outer scale of the turbulence and the scale of the physical system, while in our simulation there is no scale separation; therefore, one should use caution when applying our simulation results to the two-scale discussion of the dynamo  $\alpha$ -effect. For two-scale approach to the dynamo problem, the reader is referred to a recent work by Brandenburg (2000), which presents a detailed account of large-scale magnetic field amplification through dynamo  $\alpha$ - and  $\beta$ -effects.

#### 4. Amplification of a small-scale seed magnetic field by the turbulence

In this section, we present the numerical analysis of a seed magnetic field that is initially concentrated at a small scale,  $k = 20$ . We start from a fully developed turbulence and a magnetic impulse

$$E_b(k) = \begin{cases} e_0 & \text{for } k = 20, \\ 0 & \text{otherwise.} \end{cases} \quad (14)$$

Such an initial condition is consistent with the theoretical analysis by Kulsrud & Anderson (1992) on the amplification of weak small-scale magnetic energy, which they called *magnetic noise*. The growth of magnetic spectrum with  $e_0 = 0.001$  (Run B) is shown in Figure 7. The initial impulse-like small-scale seed magnetic field is located at  $k = 20$ . After the simulation starts, the narrow impulse quickly becomes broader and broader, extending to both larger and smaller scales than  $k = 20$ . It extends to large wave numbers (small scales) and soon hits the magnetic dissipation scale  $k_{b,D} = 28$  and the energy is removed by dissipation near  $k_{b,D}$ . The broadened, impulse-like, seed field also extends to small wave numbers, transporting magnetic energy to larger and larger scales. From  $t = 2.2$  to  $t = 19.0$ , the portion of the growing magnetic spectrum that extends from  $k = 1$  to  $k_{v,D}$  follows a  $k^{3/2}$  power law, indicated by a group of dashed lines in Figure 7. Such  $k^{3/2}$  profiles are reminiscent of the kinematic analysis of the magnetic spectrum by Kulsrud & Anderson (1992). Note that by Kulsrud & Anderson, such  $k^{3/2}$  profiles should extend into the range beyond  $k_{v,D}$  but before  $k_{b,D}$  is reached. However, because of the low resolution of our simulation, we do not have a long range between  $k_{v,D}$  and  $k_{b,D}$ ; therefore, the magnetic energy spectrum beyond  $k_{v,D}$  can be strongly affected by the dissipation process near the magnetic dissipation scale and does not exhibit the  $k^{3/2}$  scaling. Future simulations with higher resolution should be able to resolve such scaling within that range.

To study the broadening of the initial magnetic impulse, we define the following two terms

$$C_b(k) = \sum_{k-0.5 \leq |\mathbf{p}| < k+0.5} \hat{\mathbf{B}}^*(\mathbf{p}) \cdot \hat{\mathbf{Q}}(\mathbf{p}), \quad (15)$$

$$L_b(k) = \sum_{k-0.5 \leq |\mathbf{p}| < k+0.5} \hat{\mathbf{B}}^*(\mathbf{p}) \cdot \hat{\mathbf{R}}(\mathbf{p}). \quad (16)$$

Here

$$\mathbf{Q} = -\mathbf{U} \cdot \nabla \mathbf{B} \quad (17)$$

is the convection term, and  $-\mathbf{B} \cdot \mathbf{Q}$  is the energy per unit time that is transferred away from magnetic field at one location to other locations. Also,

$$\mathbf{R} = \mathbf{B} \cdot \nabla \mathbf{U} \quad (18)$$

is the term representing the line stretching effect, and  $\mathbf{B} \cdot \mathbf{R}$  is the work done to the magnetic field by the velocity field. In Figure 8, we plot  $kC_b(k)$  and  $kL_b(k)$  at different time points. At  $t = 0.2$ , panel (a) of Figure 8 shows that the magnetic energy of the impulse at  $k = 20$  is being transported to scales larger and smaller than  $k = 20$ . In panel (b) of Figure 8, the energy is being removed from  $k = 20$  to larger and smaller scales. It shows that the line stretching effect is generating magnetic structures at other scales. Panels (a) and (b) together explain the broadening of the impulse shown in Figure 7. Notice that at  $t = 0.2$ , the convection effect, i.e.,  $C_b(k)$ , is comparable to the line stretching effect, i.e.,  $L_b(k)$ . However, from panels of the right column of Figure 8, we find that the line stretching effect soon becomes dominant over the convection effect, which is shown at different times in the left column of Figure 8.  $kL_b(k)$  is non-negative at all  $k$ 's, therefore always converting kinetic energy to magnetic energy. The convection term at different  $k$ 's has different signs at different times, meaning that the magnetic energy can be transported into or out of certain scale of the MHD turbulence. Panels (b), (d), (f) and (h) also show that the line stretching effect is most prominent at small scales, that is, the scales between the velocity dissipation scale,  $k_{v,D} = 13$ , and the magnetic dissipation scale,  $k_{b,D} = 28$ .

According to Kulsrud & Anderson(1992), before the back reaction of magnetic field is strong enough to alter the velocity field, the exponential growth of magnetic energy from a magnetic impulse should be attributed to the line stretching at the velocity dissipation scale, i.e.,

$$\frac{d\mathcal{E}}{dt} = 2\gamma\mathcal{E} \quad (19)$$

where  $\gamma = 1/\tau_{max}$  is the inverse of the eddy turnover time of velocity field at dissipation scale  $k_{v,D}$ . Recent work by Chandran(1997) and Schekochihin & Kulsrud(2000) modified  $\gamma$  from  $1/\tau_{max}$  to  $\epsilon/\tau_{max}$  and  $\epsilon \approx 0.6$  is due to the non-zero correlation time of the velocity field. We have found such kinematic exponential growth stage in our simulations, such as the  $e^{\beta_1 t}$  portion of the magnetic energy growth in Figure 9. To test if the growth rate,  $\beta_1$ , in such exponential growth stage can be estimated according to the theory of Kulsrud & Anderson, we have measured this quantity from our simulation results. In Figure 10, we plot the kinematic exponential growth stage of the magnetic field, which extends from  $t = 2$  to  $t = 9$  for Run C with an  $e_0(k = 20) = 10^{-5}$ . The best fitting to  $E_b(t)$  gives a growth rate of  $\gamma_b = 0.36 \pm 0.05$ . We also calculated the growth rate due to line stretching by the largest eddies,  $\gamma_{eddy} = 0.18 \pm 0.04$ . The smallest eddy turnover time calculated from our numerical results within this time range is  $\gamma_n = 0.69 \pm 0.12$ . Therefore, in our simulation, the modification factor due to non-zero correlation time is  $\epsilon = \gamma_b/\gamma_n \approx 0.52$ , and such result is consistent with the work by Chandran (1997) and that of Schekochihin & Kulsrud (2000).

For a Kolmogoroff turbulence, the eddy turnover time at scale  $k_{v,D}$  can be calculated as

$$\tau_{Kol,D} = \tau_{eddy} \left( \frac{k_{v,D}}{k_{eddy}} \right)^{-2/3}. \quad (20)$$

With  $\tau_{eddy}$  and  $k_{eddy} \sim 1/L$  from our simulation, we have  $\gamma_{Kol,D} = 1/\tau_{Kol,D} = 0.57 < \gamma_n = 0.69$ . This is due to the fact that the hyper-viscosity flattens the kinetic energy spectrum, hence produces larger values of velocity near the dissipation scale than that in Kolmogoroff turbulence. However, the nature of the growing of the magnetic field due to line stretching near the dissipation scale does not change with the slightly flattened kinetic energy spectrum. This can be seen from the work by Kulsrud & Anderson (1992). The growth rate of magnetic energy depends on the integral

$$\gamma \propto \int k^2 J(k, 0) dk \quad (21)$$

where  $J(k, 0)$  kinetic energy density at zero frequency. For the velocity field in our simulation, we have  $J(k, 0) \sim k^{-1.2}$ , thus most of the contribution to  $\gamma$  still comes from the smallest eddies.

## 5. Discussion

Our simulations show that the interaction between fully developed, constantly forced turbulence and an initially weak seed magnetic field will always lead to the growth of magnetic field at different scales of the turbulence. Given an initially weak, large-scale external magnetic field, the emergence of magnetic energy at small scales is due to the line stretching of  $\bar{\mathbf{B}}$  by the velocity field. This is a kinematic process, as the velocity field is not affected much by the growing magnetic field. Within the inertial range, where dissipation is negligible, the magnetic field is amplified mainly by the line stretching term, i.e., the second term of equation (11). This kinematic stage finishes when the nonlinear interaction between the growing magnetic field becomes comparable to the line stretching term, and a dynamic growth stage follows. In other words, when the terms  $\mathbf{U} \cdot \nabla \mathbf{b}$  and  $\mathbf{b} \cdot \nabla \mathbf{U}$  are of the same order as  $\bar{\mathbf{B}} \cdot \nabla \mathbf{U}$ , (11) is not valid anymore, and the self-excitation of the growing magnetic field within the inertial range will dominate other amplification processes. This is shown clearly as stage 2 in Figure 4, where the total magnetic energy grows exponentially. And from Figure 5, we find that such an exponential self-excitation stage happens after the magnetic energy densities at different scales grow to be comparable to the magnetic energy density of  $\bar{\mathbf{B}}$ .

Several authors have been arguing that there might be a relation between the strength of a large-scale magnetic field,  $\bar{\mathbf{B}}$ , and the strength of the fluctuating component of the magnetic field,  $\mathbf{b}$ . Krause and Rädler (1980, chapter 7) derived a relation for 3D MHD

between  $\overline{B}^2$  and  $\langle b^2 \rangle$  in the form

$$\langle b^2 \rangle = \overline{B}^2 \frac{\eta_T}{\eta}, \quad (22)$$

where  $\eta_T$  and  $\eta$  are the turbulent diffusion coefficient and the magnetic diffusivity, respectively. The governing equation they used in their derivation of (22) was equation (11), and the nonlinear terms  $\mathbf{Q}$ ,  $\mathbf{R}$  in (17) and (18) were ignored. Our simulations show that this is not a valid procedure, as terms like  $\mathbf{Q}$  and  $\mathbf{R}$  are of importance to the exponential growth of the magnetic energy. In fact, from our simulations we find that no matter how large or small the initial large-scale magnetic field is, after  $5 - 10$  eddy turnover times of the turbulence, a statistically stationary magnetic energy spectrum will be formed.

The amplification of the small-scale seed field, simulated in Runs B and C, further shows that relation (22) is not necessarily true, as  $\overline{B} = 0$  in these two runs. The growth of magnetic field at all scales (see Figure 7) can be due only to the nonlinear interactions between the velocity field and the magnetic field at different scales.

In the two simulation runs (B & C) with a moderate magnetic Prandtl number ( $Pr = 3$ ), the magnetic energy within the inertial range,  $E_{\mathcal{I}}$ , which is initially set to zero, grows to a steady state in which  $E_{\mathcal{I}} \geq E_{\mathcal{D}}$ , where  $E_{\mathcal{D}}$  is the magnetic energy stored between the two dissipation scales,  $k_{v,D}$  and  $k_{b,D}$  (see Table 1 for more details). Some authors (Cowley 2000) argue that for large magnetic Prandtl number, the magnetic field at small scales, i.e.,  $k_{v,D} \leq k \leq k_{b,D}$ , grows so fast and strong that it swamps the velocity field at all scales and the magnetic field within the inertial range cannot grow at all. Our simulation, which includes both the inertial range and the dissipation range, does not support such picture. Instead, our simulation shows that  $E_{\mathcal{I}}$  does grow. The initial magnetic impulse at small scales spreads to all scales between  $k_{v,D}$  and  $k_{b,D}$ . The growth rate of magnetic energy at these small scales is approximately the inverse of the eddy turnover time of the smallest

turbulence eddies, as predicted by Kulsrud & Anderson (1992). During this kinematic growth period, the magnetic energy spectrum is peaked near  $k_{b,D}$ , and extends into the inertial range with a profile of  $\sim k^{3/2}$ , providing seed magnetic field in the inertial range. Such seed magnetic field does grow, and the growth rate in the kinematic growth period is  $\propto 1/\tau_{max}$ . Let range  $\mathcal{D}$  include all the scales between  $k_{v,D}$  and  $k_{b,D}$  (see Table 1 for definitions of other terms). As the magnetic field within range  $\mathcal{D}$  continues to grow, it starts to exert strong back reaction on the velocity field near scale  $k_{v,D}$  and suppresses it. This starts the dynamic growth period of the magnetic field. The eddy turnover time  $\tau_{max}$  of the gradually suppressed velocity field increases, which reduces the growth rate,  $\beta_{\mathcal{D}} \sim 1/\tau_{max}$ , of the magnetic field within range  $\mathcal{D}$ . Because  $\beta_{\mathcal{D}}$  is reduced, the back reaction of the magnetic field near the scales  $\sim k_{v,D}$  on the velocity field is reduced, too. For the forced turbulence, line stretching in range  $\mathcal{I}$  (the inertial range, see Table 1) is still in effect as the velocity field in this range is not completely suppressed by the growing magnetic field. Therefore, the magnetic field within the inertial range continues to grow at a rate smaller than  $1/\tau_{max}$  but not smaller than  $1/\tau_{eddy}$ . The growth rate of the total magnetic energy during the dynamic growth stage is a combination of the growth rates of  $E_{\mathcal{I}}$  and  $E_{\mathcal{D}}$ , as shown as the  $e^{\beta_2 t}$  stage of Figure 9. In Figure 11, we compare the growth history of  $E_{\mathcal{I}}$  and  $E_{\mathcal{D}}$ . Let  $\mathcal{E} = E_{\mathcal{I}} + E_{\mathcal{D}}$ ,  $R_i = E_{\mathcal{I}}/\mathcal{E}$  and  $R_d = E_{\mathcal{D}}/\mathcal{E}$ . Figure 11 shows that  $E_{\mathcal{I}}$  starts from 0, and continues to grow until it dominates  $E_{\mathcal{D}}$  after  $t \sim 40$ . In previous numerical simulations (Kinney *et al.* 2000),  $E_{\mathcal{I}}$  was not considered at all, and the growth of  $\mathcal{E}$  is attributed only to  $E_{\mathcal{D}}$ . Figure 11 shows that  $E_{\mathcal{I}}$  is as important as  $E_{\mathcal{D}}$  in the amplification process of the magnetic field in turbulence, hence it must be included in numerical studies.

We also studied a relevant process in Run D. The initial seed magnetic field is composed of two components: a large-scale magnetic field,  $\overline{\mathbf{B}}$ , and a small-scale magnetic field  $\mathbf{B}_{k=20}$  that is initially concentrated at  $k = 20$ . The growth of the magnetic energy spectrum given

such combined initial conditions is shown in Figure 12. For this simulation run, we set the initial magnetic energy density of  $\bar{\mathbf{B}}$  equal to that of  $\mathbf{B}_{k=20}$ , so that we can compare the contributions of these two initial seed fields to the growth of the magnetic energy at each  $k$ . Figure 12 shows that both  $\bar{\mathbf{B}}$  and  $\mathbf{B}_{k=20}$  contribute to the amplification of magnetic field at each scale. For a certain  $k$  within the inertial range, these two contributions to the magnetic energy density at this scale race against each other: the contribution from  $\bar{\mathbf{B}}$  initially grows as  $\sim t^2$ , followed by an exponential growth  $\sim e^{t/\tau_{eddy}}$ ; the contribution from  $\mathbf{B}_{k=20}$  grows initially as  $\sim e^{t/\tau_{max}}$ , followed by another near-exponential growth with a smaller growth rate. The growth rate of magnetic energy density within the inertial range is greater than both of the growth rates in Run A and Run B, and this is because in Run D, both the large-scale and small-scale magnetic fields provide seed field within the inertial range. We believe this model can be applied to many real astrophysical systems, for example, in the regions where supernova remnants mix with ambient interstellar medium. Supernova remnants usually carry small-scale magnetic field, while the ambient interstellar medium can be threaded by large-scale magnetic field. Both the initial large-scale magnetic field in the interstellar medium and the small-scale seed magnetic field in supernova remnants will contribute to the growth of magnetic field at different scales. It is also possible that in the early evolution stages of galaxies, the seed magnetic field may have components of both large and small scales. As we have shown in above discussions, because the contributions of these two components to the amplification of magnetic field at different scales are different, we have to treat both of them in discussions of dynamo action in galaxies.

Scale separation, which is discussed extensively in Brandenburg (2000), is not considered in this work. What we mean by “large scale” in this work is the scale  $k \rightarrow 0$ , while the “large scale” in Brandenburg (2000) is  $k \sim 1$ . That is, there are no scales between the large scale  $S$  and the forcing scale  $k \sim 1$  in this work. We force the turbulence near

$k = 1$ , which is near the size of the simulation box, while the forcing scale of Brandenburg (2000) is  $k = 5$ . However, we did find the scale-by-scale growth of magnetic energy in our simulation. In the first two cases of our simulation (Runs A, B and C), in the kinematic development stage, magnetic energy near the kinetic dissipation scale is always stronger than the magnetic energy at different scales of the inertial range. When the magnetic field is amplified, the effect of back reaction first comes in near the kinetic dissipation scale and the growth of magnetic energy near that scale first slows down. After the slowing down of magnetic energy growth first appears near  $k_{v,D}$ , the energy growth at the scale that is slightly larger than the dissipation scale starts to slow down, followed by the energy growth slowing down at even larger scales (or smaller  $k$ 's). Such slowing down, which starts from  $k_{v,D}$ , continues from the dissipation scale and moves from right to left in  $k$ –space, until the magnetic energy near the forcing scale stops growing. Then, the development enters fully saturated stage, with the magnetic energy at different scales fluctuating around their saturated values. Such successive slowing down of magnetic energy growth from the kinetic dissipation scale to the forcing scale is due to the effect of back reaction of the growing magnetic field on the velocity field, and such effect of back reaction comes in scale-by-scale, starting from  $k_{v,D}$ . Note that this is different from the energy growth near scales  $k < 5$  in the work by Brandenburg (2000, Fig. 18) in the following sense: because the author is studying the dynamo  $\alpha$ – and  $\beta$ –effects, scale separation is necessary as the author compares the numerical results with the prediction of theoretical two-scale approach to the problem. In that work, the growth of magnetic field at  $k < 5$  is mainly due to an  $\alpha$ –effect, through which the helical velocity field aligns the magnetic field within the scales from  $k \sim 5$  (i.e., the forcing scale) down to  $k_{v,D}$  (i.e., the kinetic dissipation scale) in such way that the magnetic field at scale  $k \sim 1$  is formed. In this work, on the other hand, the growth and the saturation of magnetic energy density at different scales is due to the interplay

between the magnetic field line stretching by the turbulent velocity field and the magnetic back reaction on the velocity field.

## 6. Conclusions and future work

We have carried out numerical simulations of 3D incompressible MHD with a magnetic Prandtl  $Pr \approx 3$ . Both the initial large-scale seed magnetic field and the initial small-scale seed magnetic field can be amplified. For a large-scale seed magnetic field, the magnetic energy density grows as  $\sim t^2$  for the first few turbulence eddy turnover times, followed by an exponential growth, of which the growth rate is  $\propto 1/\tau_{eddy}$ . For a seed magnetic field at an initial input small scale, during the kinematic development stage, magnetic energy can be transported to all scales larger and smaller than the initial input scale: near the magnetic dissipation scales magnetic energy is removed by magnetic resistivity, while from the outer scale of the turbulence to the initial input scale, the magnetic energy spectrum follows a profile of  $\sim k^{3/2}$ . The measurement of the growth rate during this kinematic process confirms the theoretical prediction by Kulsrud & Anderson (1992) that the kinematic growth rate is  $\propto 1/\tau_{max}$  where  $\tau_{max}$  is the eddy turnover time of the smallest eddies of the turbulence. Entering the dynamic growth stage, the growth of magnetic field at small scales exerts a strong back reaction on the velocity field near the velocity dissipation scale. The suppression of the velocity field slows down the growth of magnetic field between the velocity dissipation scale and the magnetic dissipation scale. However, the magnetic field within the inertial range of the forced turbulence continues to grow. The magnetic field within the inertial range grows to a steady state that has a profile  $\sim k^{-1}$  between the forcing scale and the magnetic dissipation scale. The contribution to the total magnetic energy from the magnetic field within the inertial range dominates that from the

magnetic field between the velocity dissipation scale and the magnetic dissipation scales. For real astrophysical systems, the initial seed magnetic field may have both a large-scale component and a small-scale component, and they would both contribute to the growth of magnetic field at all turbulence scales.

Our simulations may suffer from the relatively low resolution ( $64^3$ ); therefore, the results may not completely applicable to very large magnetic Prandtl cases. The low resolution forces us to adopt the hyper-viscosity  $\nu_7$  and the hyper-resistivity  $\lambda_7$  in a few runs of our simulation. Although the introduction of hyper-viscosity and hyper-resistivity does not change the fundamental physics of our discussion given above, the simulation results, such as our estimates of the growth rates, can be slightly different from the results obtained from simulation runs with normal viscosity and normal resistivity, as we have discussed in Section 4. Nevertheless, our simulations show at least that the inertial range of the turbulence must be included in the discussion of how the growing small-scale magnetic field affects the growth of magnetic field at all scales of the turbulence. This is of paramount importance to the correct understanding of astrophysical dynamo processes. In future work, we expect to study the growth of magnetic field at all turbulence scales with larger numerical resolutions.

I am very grateful to Prof. George B. Field and Prof. Eric G. Blackman for many stimulating discussions. I also thank an anonymous referee for many valuable and insightful comments. I benefited from my discussions with Axel Brandenburg, Ben Chandran, Steve Cowley, Hantao Ji, Russell Kulsrud, Keith Moffatt and Jason Moran. I also want to thank the organizers and all participants of the Astrophysical Turbulence Conference held at ITP of UC Santa Barbara, from May 8 to May 12, 2000.

## REFERENCES

Brandenburg, A. 2000, preprint, astro-ph/0006186 v2

Canuto, C., Hussaini, M. Y., Quarteroni, A. & Zang, T. A. 1988, *Spectral Methods in Fluid Dynamics*, (Berlin Heidelberg: Springer-Verlag Press)

Chandran, B. D. G. 1997, ApJ, 482, 156

Chen, S., Doolen, G. D., Kraichnan, R. H. & She, Z-S 1993a, Phys. Fluids, A, 5(2), 458

Chen, S., Doolen, G. D., Herring, J. D., Kraichnan, R. H., Orszag, S. A. & She, Z-S 1993b, Phys. Rev. Lett., Vol. 70, Num. 20, 3051

Cho, J. & Vishniac, E. T. 2000, preprint, astro-ph/0003404

Cowley, S. 2000, *Dynamos in Galaxies*, presented to *Astrophysical Turbulence* conference.  
(see [http://online.itp.ucsbg.edu/online/astrot\\_c00/cowley/](http://online.itp.ucsbg.edu/online/astrot_c00/cowley/))

Kinney, R.M., Chandran, B. D. G., Cowley, S. & McWilliams, J.C. 2000, preprint

Krause, F. & Rädler, K.H. 1980, Mean-Field Magnetohydrodynamics and Dynamo Theory,  
(Oxford: Pergamon)

Kulsrud, R.M. & Anderson, S.W. 1992, ApJ, 396, 606

Machiels, L. & Deville, M. O., 1998, J. Comput. Phys., 145, 246

Moffatt, H.K. 1978, *Magnetic Field Generation in Electrically Conducting Fluids*  
(Cambridge: Cambridge University Press)

Parker, E. N. 1979, *Cosmical Magnetic Fields* (Oxford: Clarendon Press)

Piddington, J. H. 1975, Ap. & Sp. Sci., 35, 269

Schekochihin, A. & Kulsrud, R. 2000, preprint, astro-ph/0002175

Table 1. Terms Used in This Paper and Their Physical Meanings

What we call	What we mean
large scale	scale $\sim S$ , which $\rightarrow \infty$ (or $k_S \rightarrow 0$ ) in this work
small scale	a scale that is between $k_{v,D}$ and $k_{b,D}$
outer scale of the turbulence	scale $\sim L$
forcing scale	scale $\sim L$
inertial range or range $\mathcal{I}$	scales between $L$ and $l_{v,D}$
range $\mathcal{D}$	scales between $l_{v,D}$ and $l_{b,D}$ ( $k_{v,D} < k < k_{b,D}$ )
$E_{\mathcal{I}}$	magnetic energy density of range $\mathcal{I}$
$E_{\mathcal{D}}$	magnetic energy density of range $\mathcal{D}$
$E_{v(b)}(t)$	history of kinetic (magnetic) energy density evolution
$E_{v(b)}(k)$	kinetic (magnetic) energy spectrum
$\overline{E}_B$	magnetic energy density of $\overline{\mathbf{B}}$
$e_0(k)$	magnetic energy density that is concentrated at scale $k$

Table 2. Measurements of various physical quantities in different simulation runs

Run	$\overline{E}_B$	$e_0(k)$	$\nu$	$\lambda$	$Pr$	$k_{v,D}$	$k_{b,D}$
A	$5 \times 10^{-4}$	–	hyper, $\nu_7 = 5 \times 10^{-16}$	hyper, $\lambda_7 = 3 \times 10^{-20}$	3	13	28
B	–	$1 \times 10^{-3}$	hyper, $\nu_7 = 5 \times 10^{-16}$	hyper, $\lambda_7 = 3 \times 10^{-20}$	3	13	28
C	–	$1 \times 10^{-5}$	hyper, $\nu_7 = 5 \times 10^{-16}$	hyper, $\lambda_7 = 3 \times 10^{-20}$	3	13	28
D	$1 \times 10^{-3}$	$1 \times 10^{-3}$	hyper, $\nu_7 = 5 \times 10^{-16}$	hyper, $\lambda_7 = 3 \times 10^{-20}$	3	13	28
E	$5 \times 10^{-2}$	–	normal, $\nu = 0.01$	normal, $\lambda = 0.01$	1	16	16
F	$5 \times 10^{-5}$	–	normal, $\nu = 0.013$	normal, $\lambda = 0.013$	1	13	13

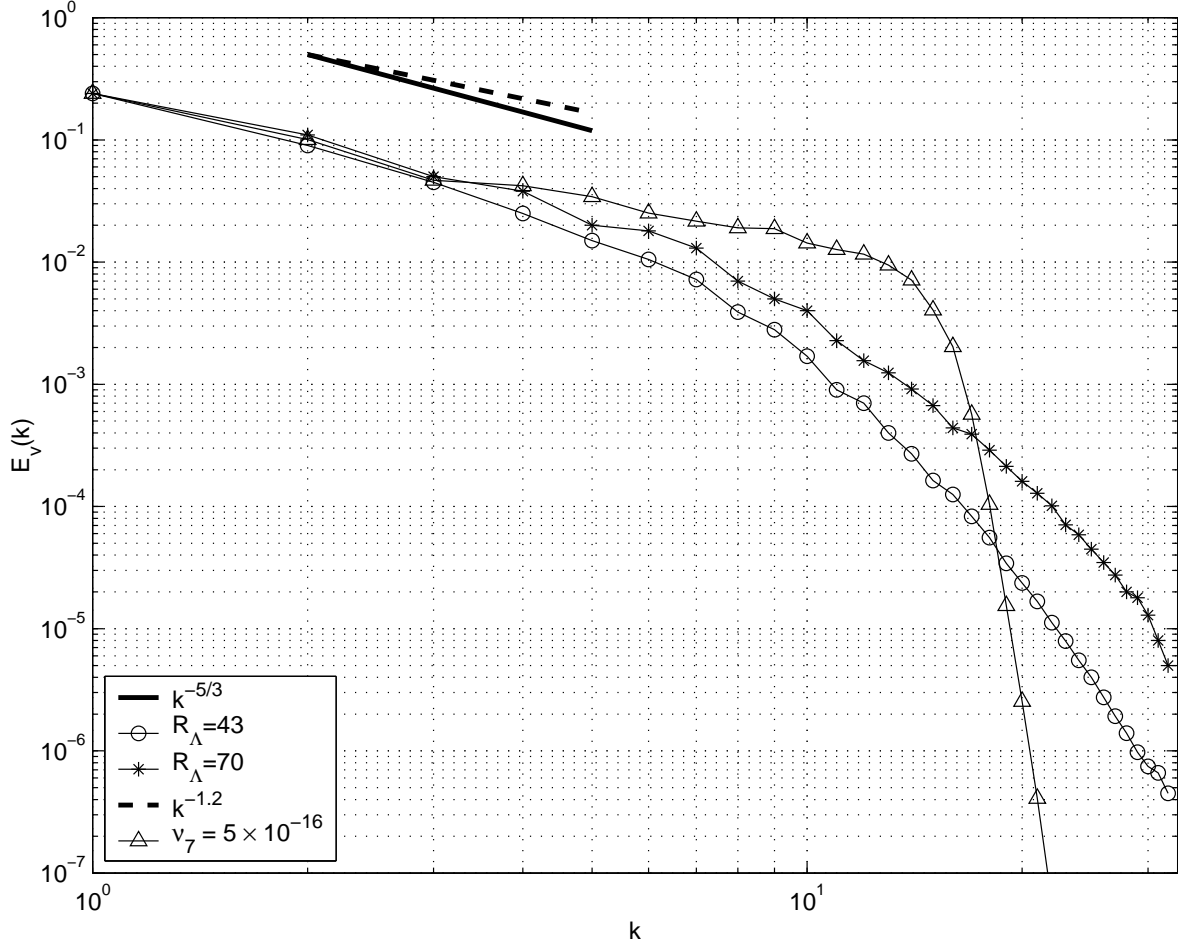


Fig. 1.— Kinetic energy spectrum at  $R_\Lambda = 43$  (circles) and  $R_\Lambda = 70$  (stars) from pure hydrodynamic turbulence simulation with a resolution of  $64^3$ . We used normal dissipation,  $\nu \nabla^2 \mathbf{U}$ , for these two runs. Also shown in this figure is the kinetic energy spectrum with a hyper-viscosity  $\nu_7 = 5.0 \times 10^{-16}$  (triangles), from a  $64^3$  spectral simulation of pure hydrodynamic turbulence.

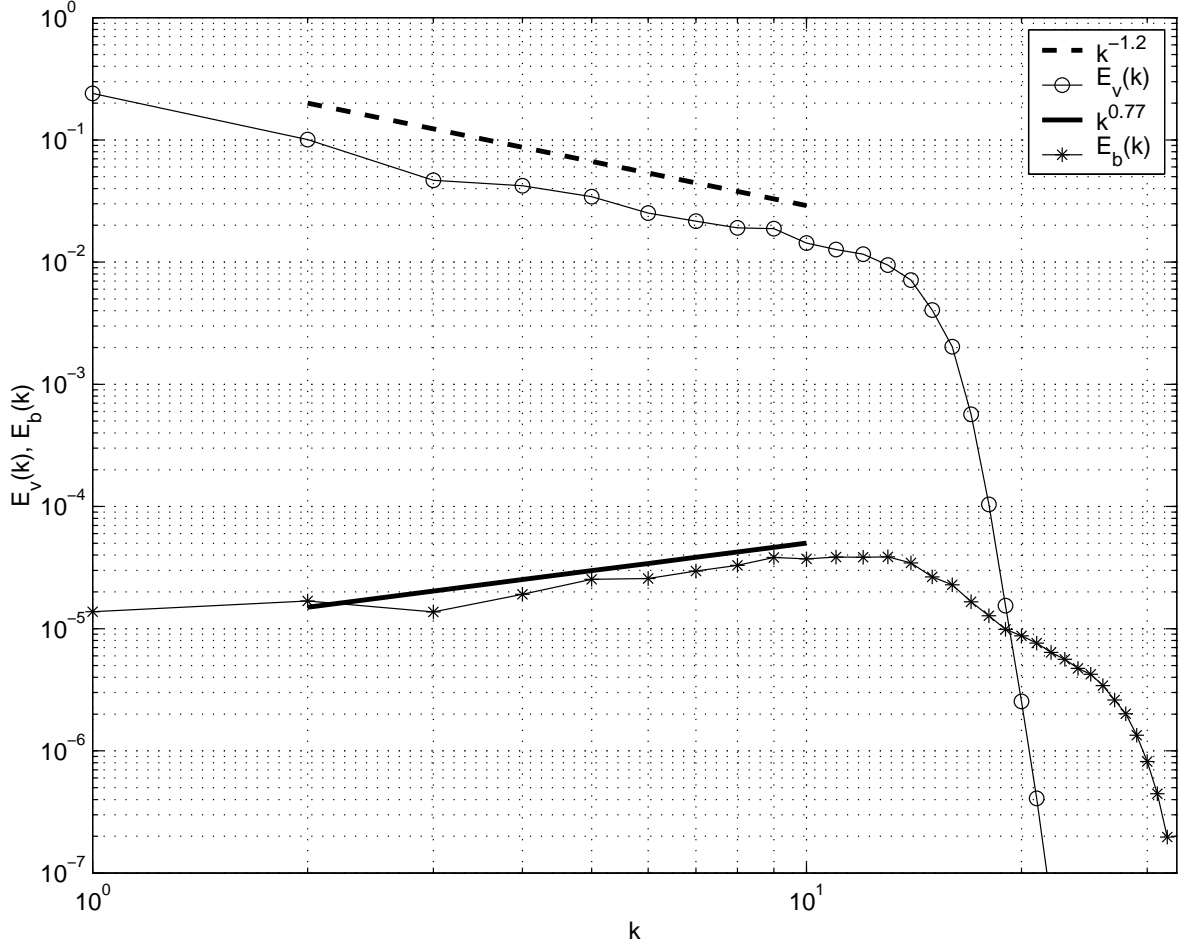


Fig. 2.— Kinetic energy spectrum  $E_v(k)$  and magnetic energy spectrum  $E_b(k)$  at  $t = 0.3$  for Run A, in which the initial large-scale seed magnetic field is  $\bar{\mathbf{B}} = \bar{B}\hat{\mathbf{e}}_y$  with a  $\bar{B} = 0.0316$ . Both axes are plotted in logarithmic scales. For a kinetic energy spectrum of the form  $k^{-p}$ , the magnetic energy spectrum, which is generated from the interaction between the turbulence and  $\bar{\mathbf{B}}$ , follows  $k^{-p+2} \sim k^{0.77}$ .

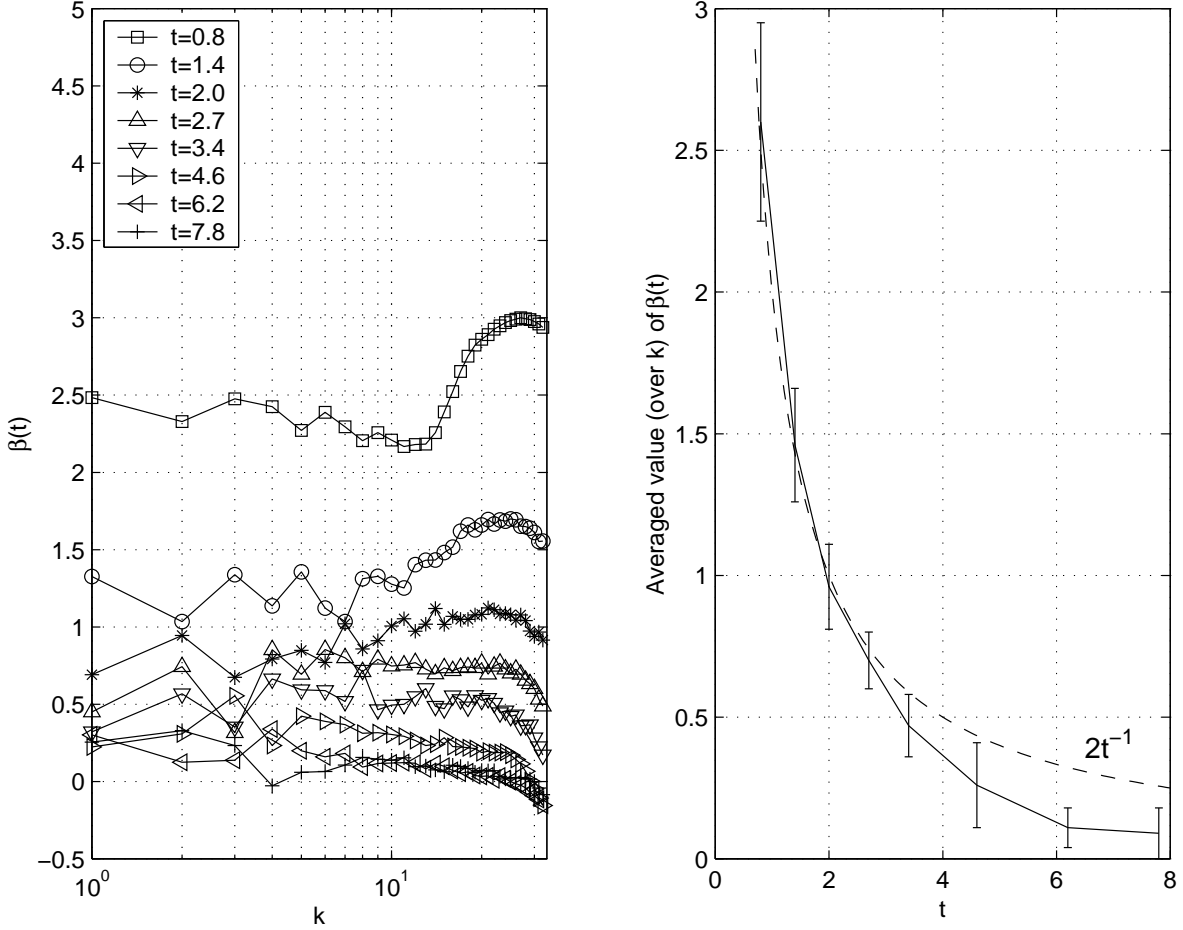


Fig. 3.—  $\beta(t)$ , as defined in equation (13) in main text, at various times are plotted in the left panel of this figure. The averaged value (over wavenumber  $k$ ) of  $\beta(t)$  as a function of time is plotted in the right panel. In the left panel, the horizontal axis is plotted in logarithmic scale, while the vertical axis is plotted in linear scale. In the right panel, both axes are plotted in linear scales. Data shown here are from Run A, in which the initial large-scale seed magnetic field is  $\bar{\mathbf{B}} = \bar{B}\hat{\mathbf{e}}_y$  with a  $\bar{B} = 0.0316$ .

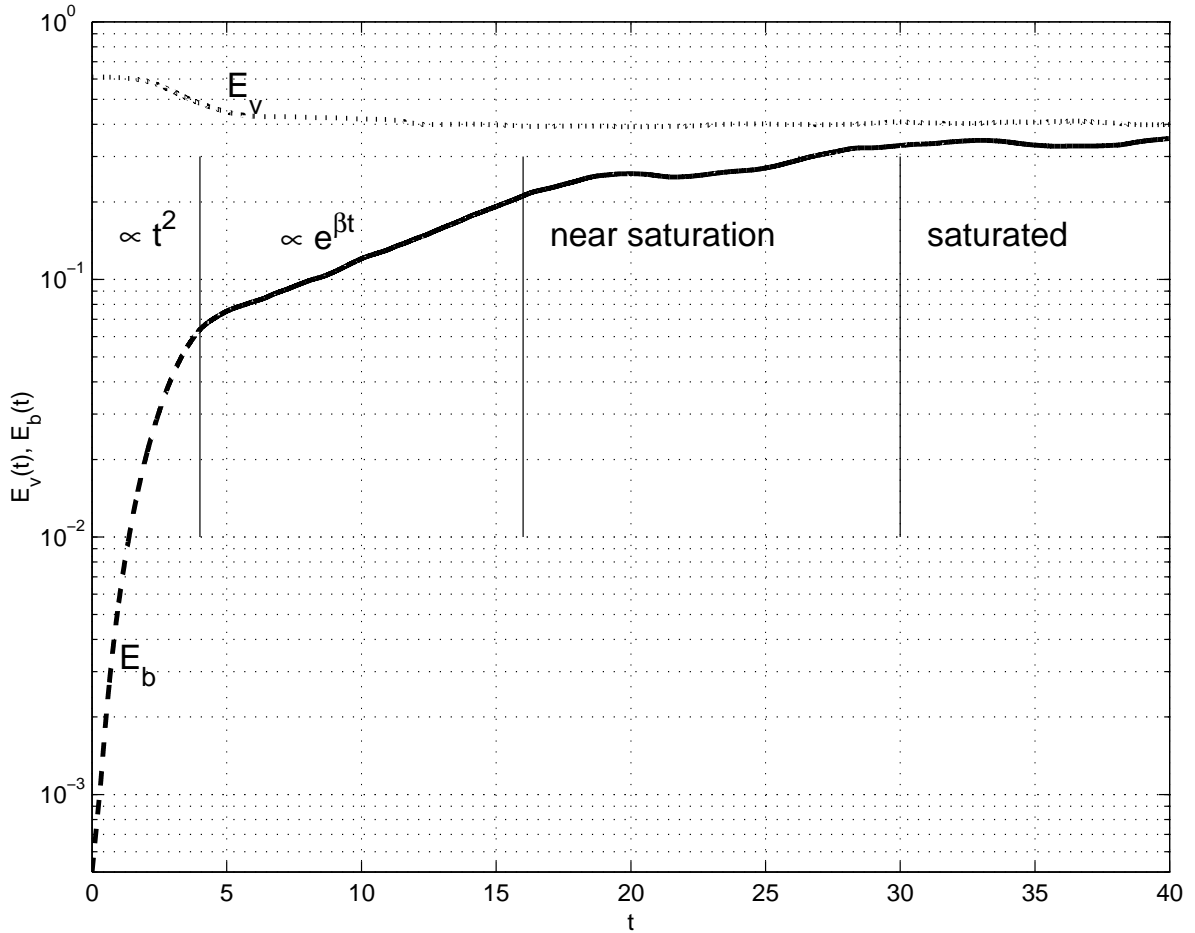


Fig. 4.— Kinetic energy density  $E_v = \sum_k E_v(k)$  and magnetic energy density  $E_b = \sum_k E_b(k)$  as functions of time. Same conditions as Figure 3. The growth of magnetic energy density follows four stages. Stage 1 starts from the beginning of the simulation to  $t = 3$ , during which the magnetic energy grows as  $t^2$ . During stage 2 that lasts from  $t = 4$  to  $t = 16$ , it grows exponentially with growth rate  $\beta = 0.1$ . After the exponential growth stage, magnetic energy density growth enters a near saturation stage from  $t = 16$  to  $t = 30$ , where the growth is further slowed down. For the saturation stage, the magnetic energy density fluctuates around 0.33, while the kinetic energy density fluctuates around 0.4.

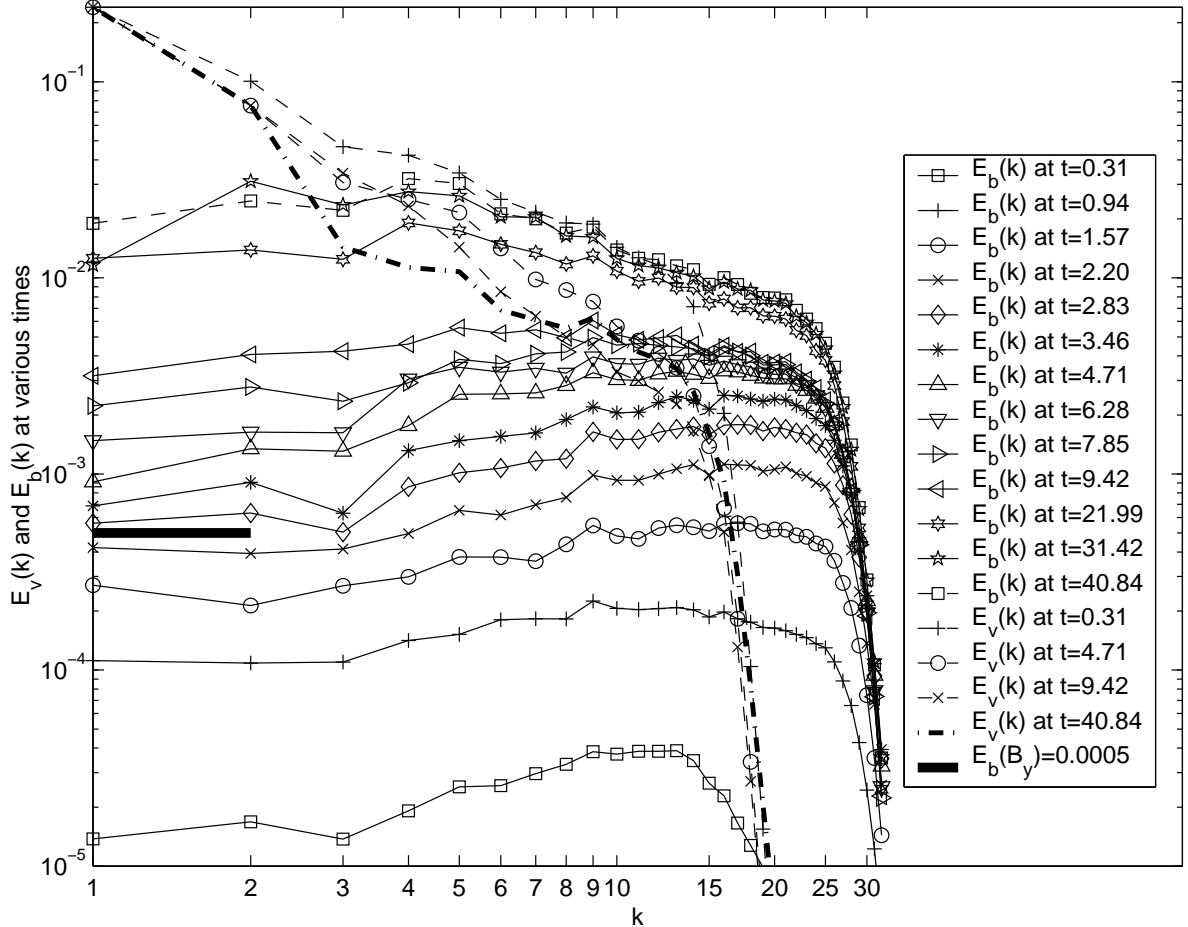


Fig. 5.— Kinetic energy spectrum  $E_b(k)$  and magnetic energy spectrum  $E_v(k)$  at different times. Data shown here are from Run A, in which the initial large-scale seed magnetic field is  $\bar{\mathbf{B}} = \bar{B}\hat{\mathbf{e}}_y$  with a  $\bar{B} = 0.0316$ . The thick horizontal line denotes the energy density due to  $\bar{\mathbf{B}}$ . Growth of the magnetic field at all scales can be seen. The growing magnetic field suppresses the velocity field in the first three stages defined in Figure 4.

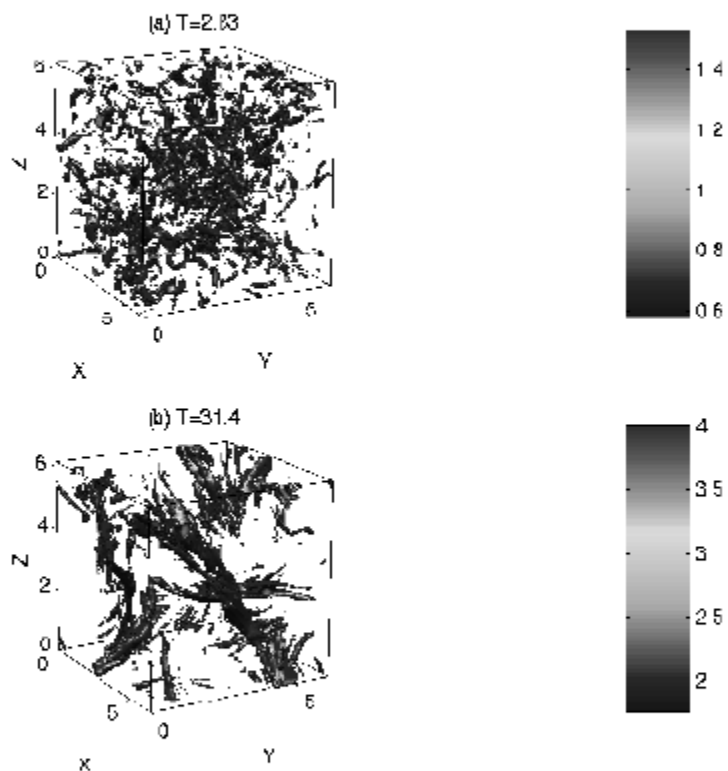


Fig. 6.— Isosurface of magnetic field magnitude at different times. The data are from Run A, in which the initial large-scale seed magnetic field is  $\overline{\mathbf{B}} = \overline{B}\hat{\mathbf{e}}_y$  with a  $\overline{B} = 0.0316$ . The isosurfaces are determined at  $2.5 \times \text{mean}\{|B|\}$ , where  $\text{mean}\{|B|\} = 0.23$  for (a) and  $\text{mean}\{|B|\} = 0.70$  for (b). The emergence of magnetic structures of the size of the simulation

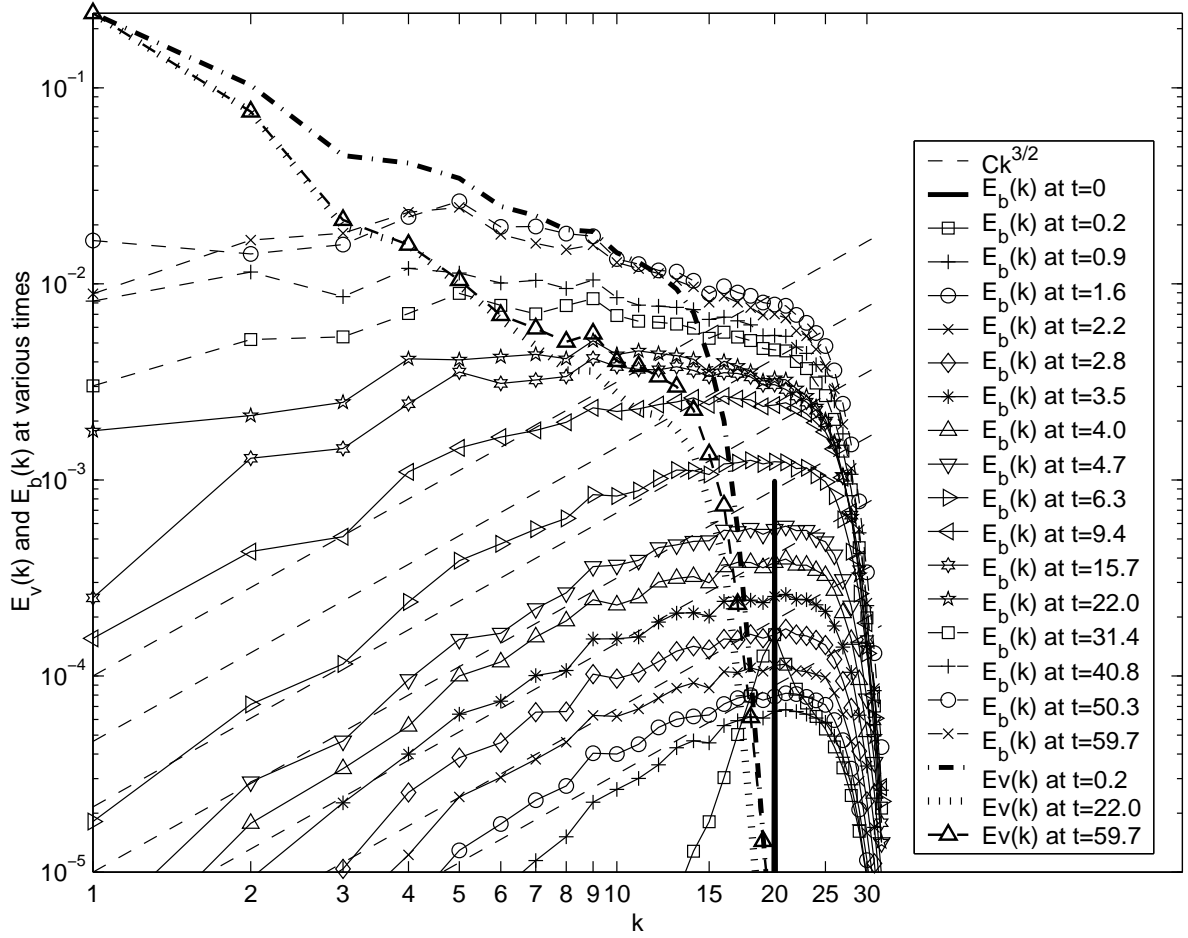


Fig. 7.— Magnetic energy spectrum  $E_b(k)$  and kinetic energy spectrum  $E_v(k)$  at various times. Data shown here are from Run B, in which an initial seed magnetic energy is concentrated at  $k = 20$  with an  $e_0 = 1 \times 10^{-3}$ . Dashed lines are  $Ck^{3/2}$  ( $C$  varies), which is reminiscent of the prediction by Kulsrud & Anderson(1992) for the magnetic spectrum that grows from a magnetic impulse.

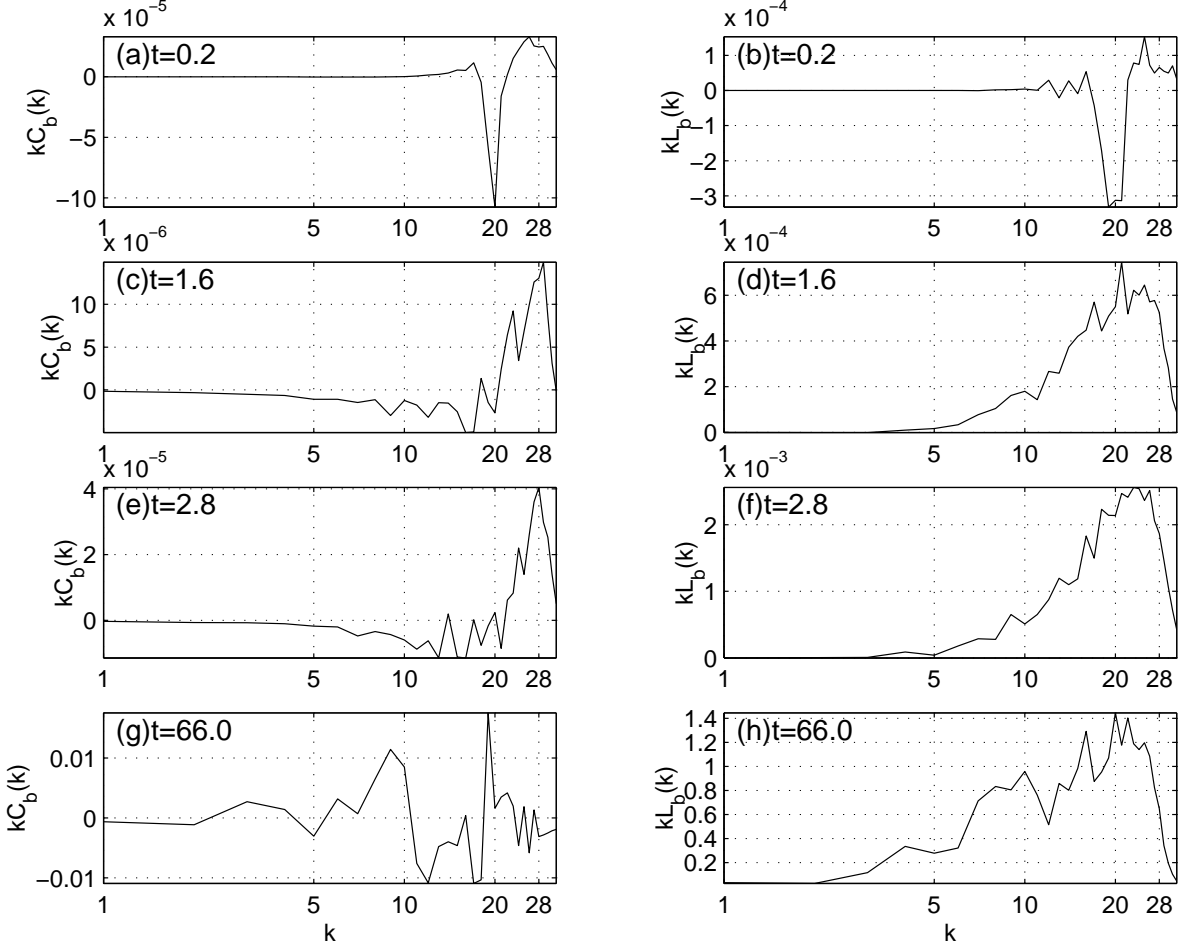


Fig. 8.— Plots of the convective effect  $kC_b(k)$  and the linear stretching effect  $kL_b(k)$  at different time points. The horizontal axis is plotted in logarithmic scale, and the vertical axis is plotted in linear scale. Data shown here are from Run B, in which an initial seed magnetic energy is concentrated at  $k = 20$  with an  $e_0 = 1 \times 10^{-3}$ . Note the different scales of  $y$ -axes of different panels.

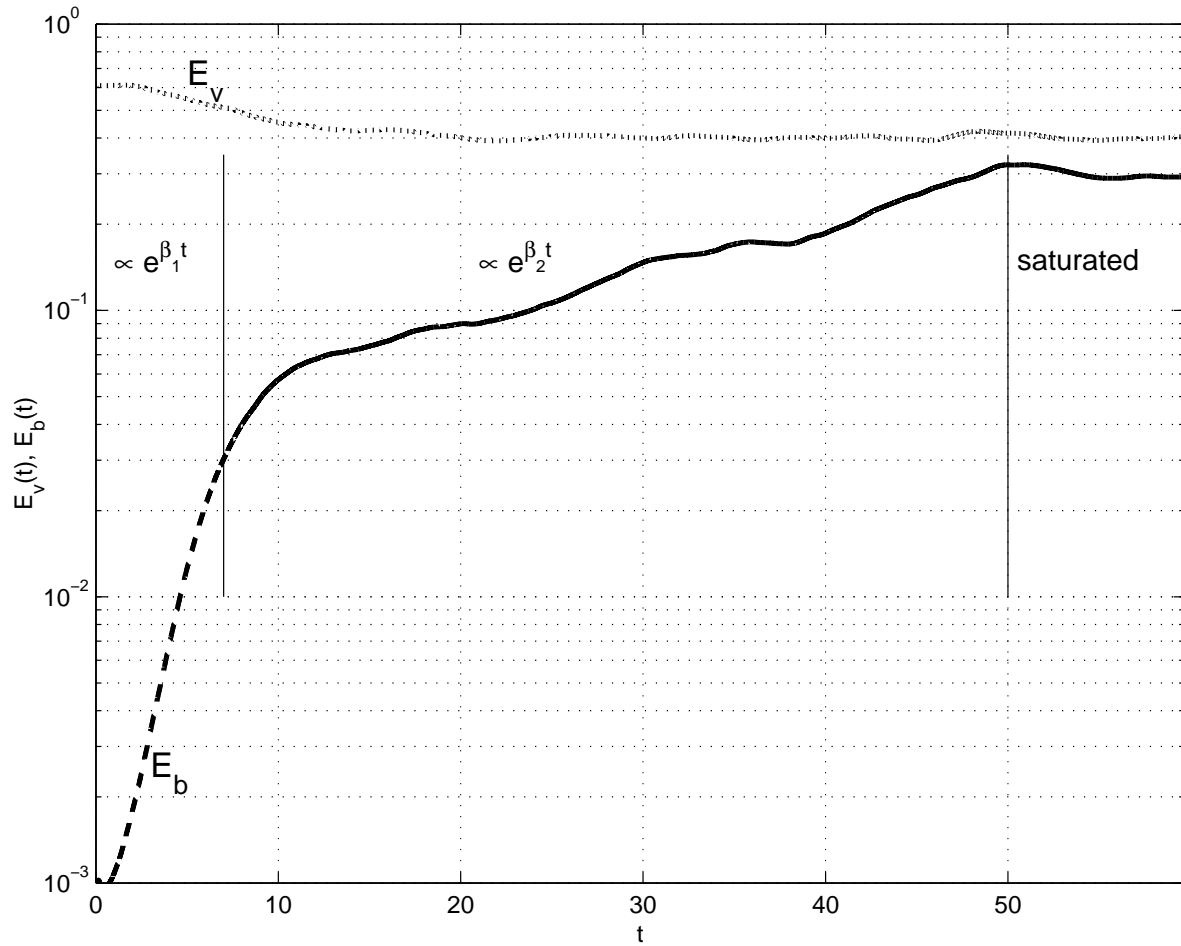


Fig. 9.— Temporal evolution of kinetic energy density and magnetic energy density. Data shown here are from Run B, in which an initial seed magnetic energy is concentrated at  $k = 20$  with an  $e_0 = 1 \times 10^{-3}$ .

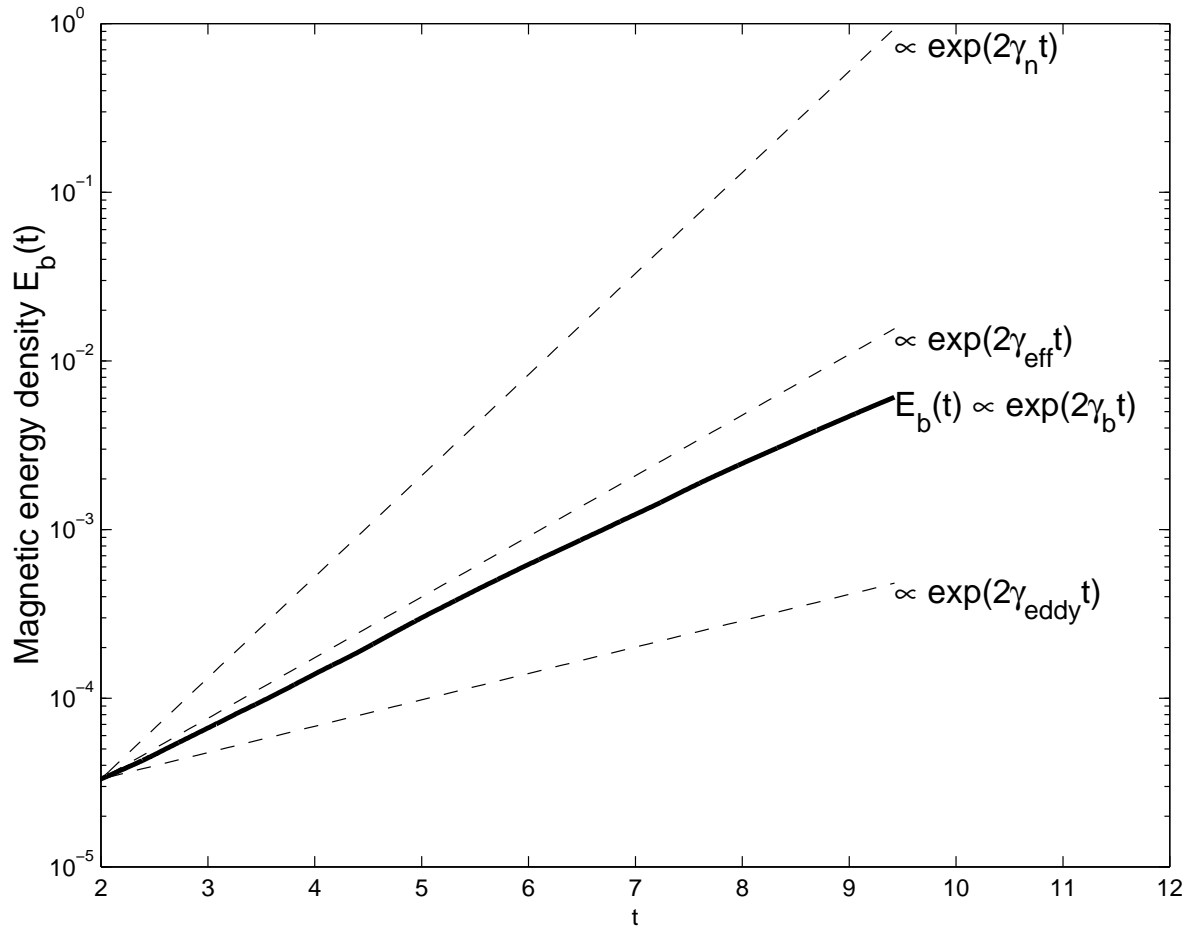


Fig. 10.— Magnetic energy density  $E_b = \sum_k E_b(k)$  as a function of time during the exponential growth stage of Run C, in which an initial seed magnetic energy is concentrated at  $k = 20$  with an  $e_0 = 1 \times 10^{-5}$ .  $\gamma_b = 0.36$ .  $\gamma_n = 0.69$  is the inverse of turnover time of the smallest eddies.  $\gamma_{eff} = 0.6\gamma_n$  as predicted by Chandran(1997) and Schekochihin & Kulsrud(2000).  $\gamma_{eddy} = 0.18$  is the inverse of turnover time of the largest eddies.

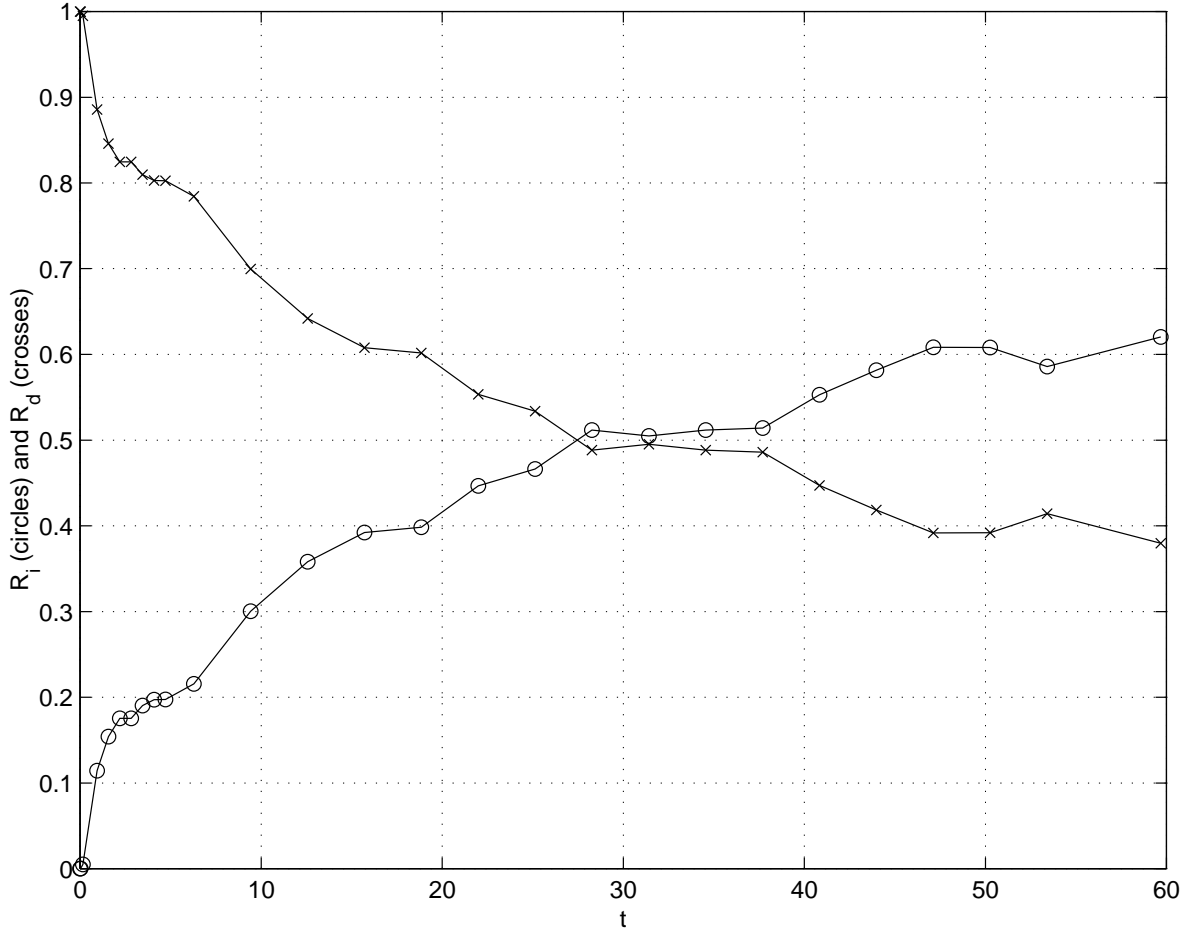


Fig. 11.— Comparison of the magnetic energy within the inertial range and the magnetic energy within the dissipation range. Note the linear-linear plot scales. Data shown here are from Run B, in which an initial seed magnetic energy is concentrated at  $k = 20$  with an  $e_0 = 1 \times 10^{-3}$ .

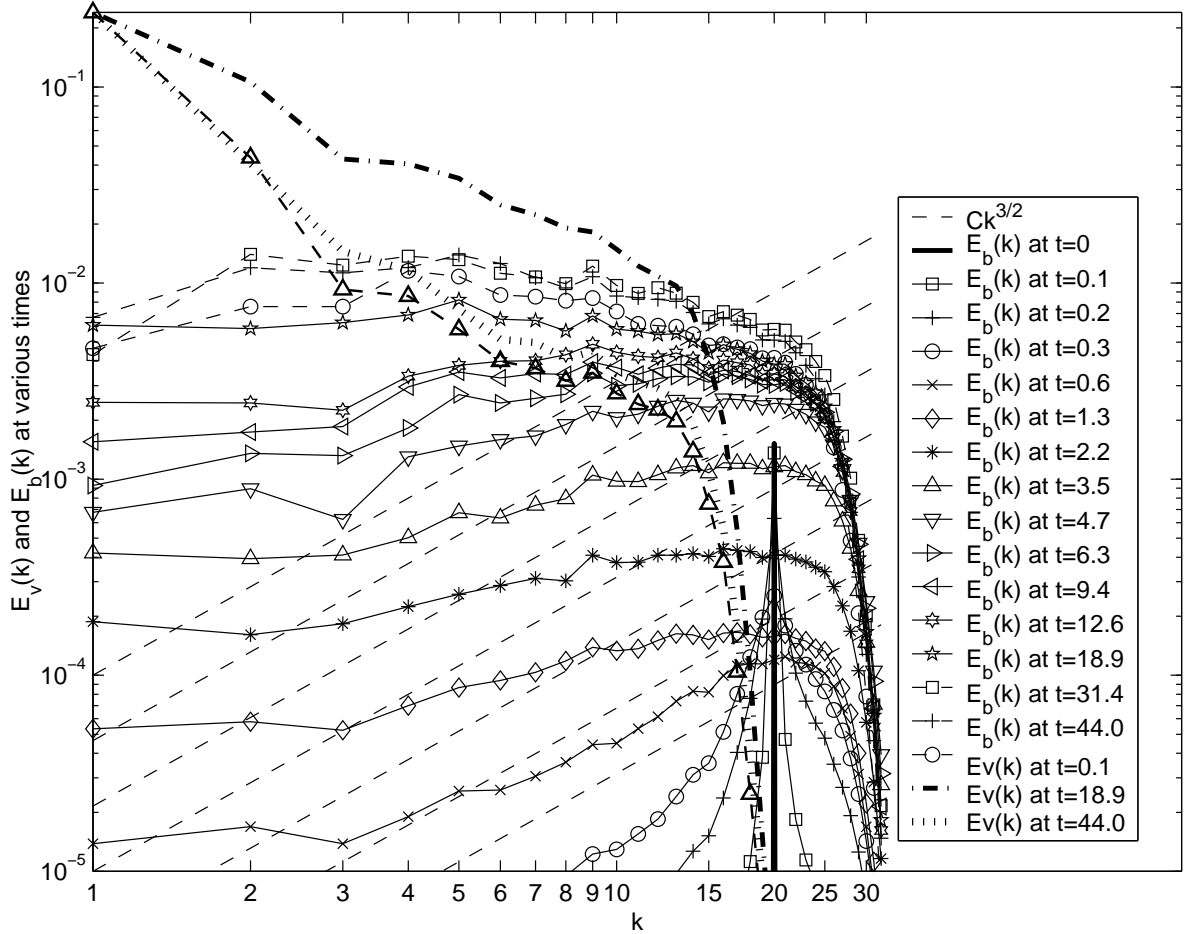


Fig. 12.— Magnetic energy spectrum  $E_b(k)$  and kinetic energy spectrum  $E_v(k)$  at different time points. Data shown here are from Run D, in which an initial seed magnetic field is composed of a large-scale seed field,  $\bar{\mathbf{B}} = \bar{B}\hat{\mathbf{e}}_y$  with a  $\bar{B}^2/2 = 1 \times 10^{-3}$ , and a small-scale seed field that is concentrated at  $k = 20$  with an  $e_0 = 1 \times 10^{-3}$ . Straight dashed lines are  $Ck^{3/2}$  for various values of  $C$ .